Generation of Isolated Attosecond Pulses by the Harmonic Spectrum of MgO under a Three-Color Laser Pulse

Jiaqi Chen(陈家祺)[1], Wenli Jiang(蒋文丽)[2,3], Yue Qiao(乔月)[2,3*], Yujun Yang(杨玉军)[2,3*], and Jigen Chen(陈基根)[1*]

[1]*School of Materials Science and Engineering, Taizhou University, Taizhou 318000, China*
[2]*Institute of Atomic and Molecular Physics, Jilin University, Changchun 130012, China*
[3]*Jilin Provincial Key Laboratory of Applied Atomic and Molecular Spectroscopy (Jilin University), Changchun 130012, China*

(Received 10 September 2024; accepted manuscript online 9 December 2024)

This study examines the high-order harmonic radiation behavior of MgO crystals driven by combined pulses based on the numerical solution of the semiconductor Bloch equation. We found that compared with the monochromatic pulse, the MgO crystal can radiate a continuous harmonic spectrum with two platforms driven by the three-color combined pulse. The reason is that under the three-color combined pulse, the electron ionization and recombination can be effectively controlled within a half-optical cycle of the laser pulse. Using this continuous spectrum, we synthesized an isolated attosecond pulse with a duration of approximately 370 as. This study provides a new perspective on all-solid-state compact optical devices.

DOI: 10.1088/0256-307X/42/1/013201 CSTR: 32039.14.0256-307X.42.1.013201

The study of light-matter interactions is a crucial method for exploring material properties and understanding fundamental physical laws. When intense laser pulses interact with matter, high-order nonlinear optical effects generate high-order harmonic radiation.[1–10] These high-order harmonics are significant sources of coherent light in the extreme ultraviolet and soft X-ray regions.[11–13] The high-order harmonic spectrum encodes structural information about the material during the emission process, making it valuable for probing the material structure and ultrafast electron dynamics.[14–16] Furthermore, owing to the broad bandwidth of its emission spectrum, high-order harmonic generation is a key technique for producing attosecond (10^{-18} s) duration optical pulses.[17–21] Such ultrashort pulses enable high-resolution studies of electron dynamics on the attosecond timescale, providing an important tool for ultrafast measurements.

Following over a decade of intensive development, significant progress has been made in experimental research on attosecond pulses. In 2012, Zhao *et al.* achieved an isolated attosecond pulse (IAP) with a duration of 67 as using a double optical gating technique that combined polarization gating with a two-color driving field.[22] In 2017, Gaumnitz *et al.* reported the shortest IAP ever recorded, with a duration of 43 as.[23] In addition, numerous theoretical approaches have been proposed for generating ultrashort attosecond pulses using high-order harmonics. In 2010, Zou *et al.* produced attosecond pulses with durations of less than 100 as using a two-color field scheme.[24] In 2019, Han *et al.* obtained high-intensity IAPs employing spatially inhomogeneous fields.[25]

Traditionally, attosecond pulses have been primarily synthesized using gaseous media. However, since Ghimire *et al.* first experimentally observed the harmonic spectrum of ZnO crystals in 2011,[26] research has expanded to study and observe harmonic radiation in a variety of solid materials, ranging from wide band-gap dielectric materials to new zero band gap two-dimensional materials.[27–36] The discovery of solid harmonics has introduced a novel approach for generating and manipulating attosecond pulses within condensed matter systems, thereby advancing the fields of strong-field physics and attosecond science.[37] In 2019, Nourbakhsh *et al.* investigated the effects of incident laser pulse intensity, ellipticity, and crystal anisotropy on the emitted harmonics and corresponding IAPs.[38] In addition, Zhong *et al.* proposed a method for generating strong circularly polarized attosecond pulses using a relativistic two-color linearly polarized laser and solid target.[39]

From the above research, it can be observed that the characteristics of the laser pulse can affect the synthesis of the solid attosecond pulse. In this study, three-band semiconductor Bloch equations[40–45] are numerically solved to systematically study the harmonic radiation process after the interaction between the three-color combined pulse and MgO crystal in the Γ-X direction. The band structure and transition dipole moment of the MgO crystal used are consistent with those reported in Ref. [46]. In our numerical simulation, the dephasing time was 1.42 fs, and the three-color field was composed of linearly polarized femtosecond laser pulses with the same polarization direction.

*Corresponding author. Email: qiaoyue22@mails.jlu.edu.cn; yangyj@jlu.edu.cn; kiddchen@126.com

The specific form is as follows (atomic units are used in this study unless otherwise stated):

$$\begin{aligned} E(t) &= E_1(t) + E_2(t) + E_3(t) \\ &= E_1 f_1(t)\cos(\omega_1 t + \phi_1) \\ &\quad + E_2 f_2(t)\cos(\omega_2 t + \phi_2) \\ &\quad + E_3 f_3(t)\cos(\omega_3 t + \phi_3), \end{aligned} \tag{1}$$

where E_j, ω_j, f_j, and ϕ_j ($j = 1, 2, 3$) are the peak intensity, center frequency, pulse envelope, and carrier-envelope phase of the electric field of three linearly polarized laser pulses, respectively. The function of the Gaussian envelope is

$$f_j(t) = \exp[-2\ln 2(t^2/\tau_j^2)], \tag{2}$$

where τ_j ($j = 1, 2, 3$) is the full width at half maximum of three linearly polarized laser pulses. The three-color laser field is composed of 16 fs/2400 nm pulse laser with a peak amplitude of 0.01 a.u., 12.7 fs/1900 nm pulse laser with a peak amplitude of 0.006 a.u., and 8 fs/1200 nm pulse laser with a peak amplitude of 0.007 a.u.

Figure 1(a) presents the temporal profile of the electric field of the three-color pulse laser synthesis with an initial carrier-envelope phase $\phi_j = 0$ (black solid line) and the monochromatic field (red dotted line). The monochromatic field is the 16 fs/2400 nm pulse laser with a peak amplitude of 0.01 a.u., which is consistent with those of the first mid-infrared femtosecond pulse laser in the three-color field. It can be seen that the synthesized electric field exhibits characteristics of a high-power, few-cycle mid-infrared femtosecond laser, and the maximum peak intensity of the three-color field is greatly improved compared to the monochromatic field. The black solid line in Fig. 1(b) depicts the high-order harmonic emission spectrum along the Γ-X direction of a MgO crystal irradiated by the three-color field. This spectrum shows a two-platform structure with supercontinuum features on both platforms. As a comparison, the red dotted line in Fig. 1(b) indicates the high-order harmonic emission spectrum of MgO crystal irradiated by a monochromatic field. It can be clearly seen from Fig. 1(b) that the harmonic spectrum of MgO crystal driven by a monochromatic field is discontinuous, the spectral peaks are relatively discrete, and there is no second platform. In addition, due to the increase of the electric field amplitude of the superimposed synthetic field, the efficiency of the whole harmonic platform in the monochromatic field is several orders of magnitude lower than that in the three-color synthetic field.

To gain a deeper understanding of the harmonic spectrum characteristics for both the three-color combined pulse and the monochromatic pulse, we employ time-frequency analysis to examine harmonic emission times. Figures 1(c) and 1(d) present the time-frequency distributions of the total harmonic spectra under the three-color combined field and the monochromatic field, respectively. The color indicates the harmonic intensity. Under the three-color combined pulse, the emission time for the second plateau (in the range of 40–60 orders) occurs later than that for the first plateau (in the range of 10–40 orders), and the intensity of the second plateau is approximately one order of magnitude lower than that of the first plateau. Notably, harmonics in both plateaus are predominantly generated via a single quantum path, resulting in a continuous and smooth harmonic spectrum under the three-color combined pulse. In contrast, under the monochromatic pulse, the first plateau of the harmonic spectrum displays multiple emission trajectories, while no trajectories are observed for the second plateau. Consequently, the MgO crystal fails to produce a continuous spectrum under the monochromatic field.

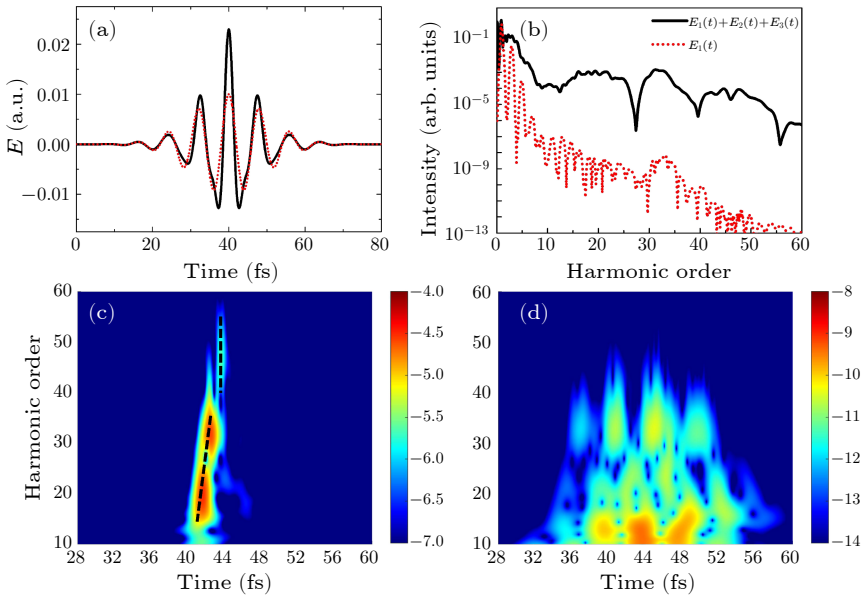

Fig. 1. (a) Variation of three-color combined pulse and monochromatic pulse with time; (b) Harmonic spectra of MgO crystal driven by three-color combined and monochromatic pulses; (c) Time-frequency distribution of total harmonic spectrum under the three-color combined pulse; (d) Time-frequency distribution of total harmonic spectrum under the monochromatic pulse.

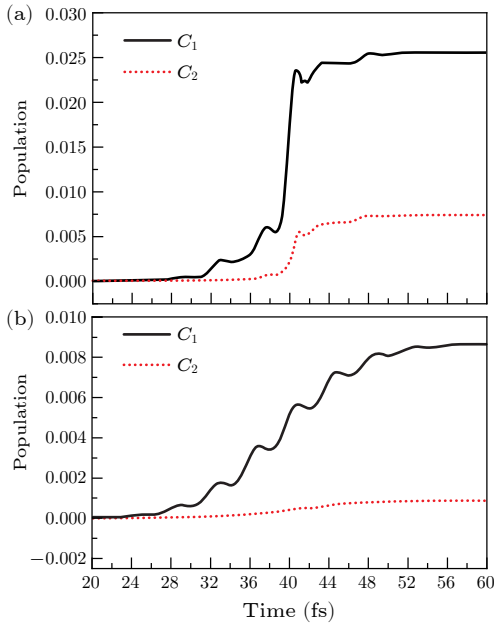

Fig. 2. Electron population in the first conduction band and the second conduction band under (a) three-color combined pulse; (b) monochromatic pulse.

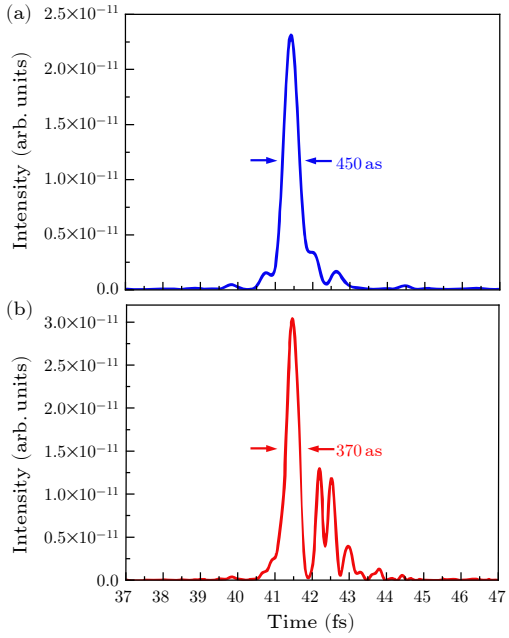

Fig. 3. Isolated attosecond pulses obtained by superposing the harmonics from (a) the 8th order to the 25th order and (b) the 8th order to the 50th order.

To elucidate the origin of the continuous spectrum emitted by MgO crystals under a three-color combined pulse, we analyze the time-dependent electron population shown in Fig. 2(a). For comparison, we also present the time-dependent electron population changes in a monochromatic field in Fig. 2(b). In the monochromatic field, electrons in the valence band undergo multiple transitions to the first conduction band, resulting in a harmonic spectrum produced through the interference of multiple emission trajectories. Additionally, the electron population in the second conduction band is minimal in the monochromatic field, indicating a low likelihood of electron transition to this band, which accounts for the weak harmonic radiation in the second plateau. Driven by the three-color combination pulse, the electrons on the valence band mainly transition to the first conduction band near the laser center, and the electrons on the second conduction band are mainly generated near the laser center, but the electrons on the second conduction band are generated slightly later than the first conduction band, so the emission time of the second platform harmonic will be later than the emission time of the first platform harmonic, so the continuous harmonic spectrum of the single quantum trajectory emission of the two platforms can be obtained under the three-color combination pulse.

The above analysis shows that the continuous harmonic spectrum obtained by using three-color combined pulses is expected to synthesize isolated attosecond pulses. In the case of the three-color field scheme, an isolated attosecond pulse with a full width at half maximum of about 450 as is obtained by superimposing 8th–25th order harmonics on the harmonic spectrum platform, as shown in Fig. 3(a). By superimposing the 8th–50th order harmonics on the harmonic spectrum platform, an isolated attosecond pulse with a weak pulse is obtained, in which the full width at half maximum of the main pulse is about 370 as, as shown in Fig. 3(b). It can be seen that efficient isolated attosecond pulse generation can be achieved by using a suitable three-pulse laser combination scheme.

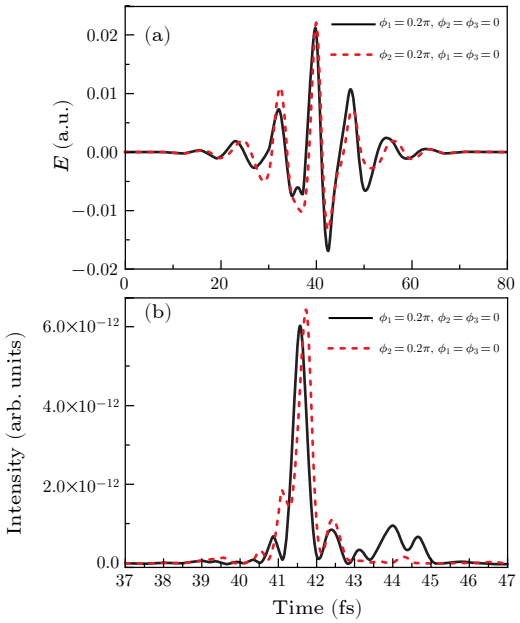

Fig. 4. (a) Variation of three-color combined pulse with time under different laser phases; (b) Isolated attosecond pulses obtained by superposing the harmonics from the 8th order to the 25th order under different laser phases.

Furthermore, we investigate the influence of the initial carrier-envelope phase of the three-color combined pulse on the attosecond pulse synthesis. Figure 4(a) shows the laser field when $\phi_1 = 0.2\pi$, $\phi_2 = \phi_3 = 0$ and $\phi_2 = 0.2\pi$, $\phi_1 = \phi_3 = 0$. It can be seen that the three-color combined pulse still exhibits few-period characteristics after chang-

ing the phase. The black solid line and the red dotted line in Fig. 4(b) show the isolated attosecond pulse obtained by superimposing the 8th–25th harmonics on the harmonic spectrum platform driven by the laser field when $\phi_1 = 0.2\pi$, $\phi_2 = \phi_3 = 0$ and $\phi_2 = 0.2\pi$, $\phi_1 = \phi_3 = 0$, respectively. It can be seen that the isolated attosecond pulse can still be obtained by changing the initial carrier-envelope phase of the laser field in a small range.

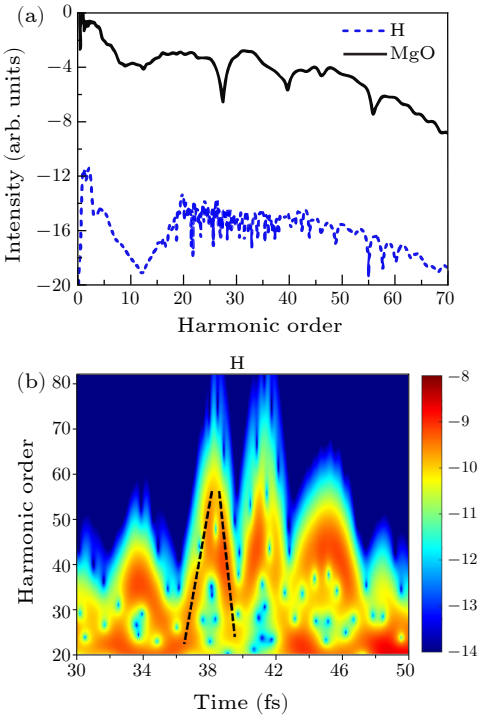

Fig. 5. (a) Comparison of harmonic spectra from H atom and MgO driven by three-color combined pulses. (b) Time-frequency emission spectra of H atom driven by three-color combined pulses.

At the end of this paper, we calculate the harmonic radiation spectrum of H atom and the corresponding time-frequency analysis spectrum under the three-color combined pulse by numerically solving the time-dependent Schrödinger equation,[47] as shown in Fig. 5. The laser parameters are consistent with those used in Fig. 1. It can be seen from Fig. 5(a) that under the same field parameters, the harmonic radiation spectrum intensity of H atom is much lower than that of MgO crystal, and the harmonic spectrum of MgO crystal is more continuous, which is more conducive to the generation of high-intensity isolated attosecond pulses. In addition, by comparing the time-frequency emission spectra of the H atom in Fig. 5(b) and the MgO crystal in Fig. 1(c), it can be found that the time-frequency emission spectrum of MgO crystal only has a single emission trajectory, which is positive chirp in the first platform and no chirp in the second platform. The time-frequency emission spectrum of the H atom has multiple emission trajectories and both positive and negative chirps.

In summary, by utilizing the interaction between a three-color combined pulse and an MgO crystal, the electron ionization is controlled to occur at a half cycle near the center of the laser pulse, we have achieved a supercontinuum spectrum with two distinct plateaus. Fourier transform is performed on the continuous harmonic spectrum to obtain an isolated attosecond pulse. The minimum pulse duration is 370 as. Since the harmonic intensity in the three-color field is higher than that in the monochromatic field, the obtained attosecond pulse intensity is relatively higher. The advantage of the three-color combined pulse lies in its ability to generate a single quantum trajectory and the isolated attosecond pulse's minimal sensitivity to the initial carrier-envelope phase. Our results highlight the potential of solids in the field of attosecond pulse synthesis and provide significant insights for the development of solid-state light sources.

Acknowledgement. This work was supported by the Natural Science Foundation of Zhejiang Province, China (Grant No. Y23A040001), the National Natural Science Foundation of China (Grant Nos. 12374029, 12074145, and 11975012), the National Key Research and Development Program of China (Grant No. 2019YFA0307700), the Research Foundation for Basic Research of Jilin Province, China (Grant No. 20220101003JC), the National College Students Innovation and Entrepreneurship Training Program (Grant No. 202310350062), the Graduate Innovation Fund of Jilin University (Grant No. 2024CX041). Yue Qiao acknowledges the High Performance Computing Center of Jilin University for supercomputer time and the high performance computing cluster Tiger@IAMP.

References

[1] Lewenstein M, Balcou P, Ivanov M Y, L'Huillier A, and Corkum P B 1994 *Phys. Rev. A* **49** 2117
[2] Kulander K C and Shore B W 1989 *Phys. Rev. Lett.* **62** 524
[3] Vampa G, McDonald C R, Orlando G, Klug D D, Corkum P B, and Brabec T 2014 *Phys. Rev. Lett.* **113** 073901
[4] Vampa G, Hammond T J, Thiré N, Schmidt B E, Légaré F, McDonald C R, Brabec T, and Corkum P B 2015 *Nature* **522** 462
[5] Yue L and Gaarde M B 2023 *Phys. Rev. Lett.* **130** 166903
[6] Goulielmakis E and Brabec T 2022 *Nat. Photonics* **16** 411
[7] Jiang S, Chen J, Wei H, Yu C, Lu R, and Lin C D 2018 *Phys. Rev. Lett.* **120** 253201
[8] Zhang C P and Miao X Y 2023 *Chin. Phys. Lett.* **40** 124201
[9] Peng Z Y, Lang Y, Zhu Y L, Zhao J, Zhang D W, Zhao Z X, and Yuan J M 2023 *Chin. Phys. Lett.* **40** 054203
[10] Lang Y, Peng Z Y, and Zhao Z X 2022 *Chin. Phys. Lett.* **39** 114201
[11] Fu Y, Nishimura K, Shao R, Suda A, Midorikawa K, Lan P, and Takahashi E J 2020 *Commun. Phys* **3** 92
[12] Heslar J, Telnov D A, and Chu S I 2017 *Phys. Rev. A* **96** 063404
[13] Zhou S S, Yang Y J, Yang Y, Suo M Y, Li D Y, Qiao Y, Yuan H Y, Lan W D, and Hu M H 2023 *Chin. Phys. B* **32** 013201
[14] He L, Yuen C H, He Y, Sun S, Goetz E, Le A T, Deng Y, Xu C, Lan P, Lu P, and Lin C D 2024 *Phys. Rev. Lett.* **133** 023201

[15] Itatani J, Levesque J, Zeidler D, Niikura H, Pépin H, Kieffer J C, Corkum P B, and Villeneuve D M 2004 *Nature* **432** 867

[16] Guo X, Jin C, He Z, Zhao S F, Zhou X X, and Cheng Y 2021 *Chin. Phys. Lett.* **38** 123301

[17] Sansone G, Benedetti E, Calegari F, Vozzi C, Avaldi L, Flammini R, Poletto L, Villoresi P, Altucci C, Velotta R, Stagira S, De Silvestri S, and Nisoli M 2006 *Science* **314** 443

[18] Agostini P and DiMauro L F 2004 *Rep. Prog. Phys* **67** 813

[19] Wang X W, Wang L, Xiao F, Zhang D W, Lü Z H, Yuan J M, and Zhao Z X 2020 *Chin. Phys. Lett.* **37** 023201

[20] Wang L, Wang X W, Xiao F, Wang J C, Tao W K, Zhang D W, and Zhao Z X 2023 *Chin. Phys. Lett.* **40** 113201

[21] Chini M, Zhao K, and Chang Z 2014 *Nat. Photonics* **8** 178

[22] Zhao K, Zhang Q, Chini M, Wu Y, Wang X W, and Chang Z H 2012 *Opt. Lett* **37** 3891

[23] Gaumnitz T, Jain A, Pertot Y, Huppert M, Jordan I, Ardana-Lamas F, and Wörner H J 2017 *Opt. Express* **25** 27506

[24] Zou P, Zeng Z, Zheng Y, Lu Y, Liu P, Li R, and Xu Z 2010 *Phys. Rev. A* **81** 033428

[25] Han J X, Wang J, Qiao Y, Liu A H, Guo F M, and Yang Y J 2019 *Opt. Express* **27** 8768

[26] Ghimire S, DiChiara A D, Sistrunk E, Agostini P, DiMauro L F, and Reis D A 2011 *Nat. Phys.* **7** 138

[27] Ndabashimiye G, Ghimire S, Wu M, Browne D A, Schafer K J, Gaarde M B, and Reis D A 2016 *Nature* **534** 520

[28] Lv Y Y, Xu J, Han S, Zhang C, Han Y, Zhou J, Yao S H, Liu X P, Lu M H, Weng H *et al.* 2021 *Nat. Commun.* **12** 6437

[29] Qian C, Yu C, Jiang S, Zhang T, Gao J, Shi S, Pi H, Weng H, and Lu R 2022 *Phys. Rev. X* **12** 021030

[30] Zhao Y T, Xu X Q, Jiang S C, Zhao X, Chen J G, and Yang Y J 2020 *Phys. Rev. A.* **101** 033413

[31] Zhao Y T, Ma S Y, Jiang S C, Yang Y J, Zhao X, and Chen J G 2019 *Opt. Express* **27** 34392

[32] Liu H, Guo C, Vampa G, Zhang J L, Sarmiento T, Xiao M, Bucksbaum P H, Vučković J, Fan S, and Reis D A 2018 *Nat. Phys.* **14** 1006

[33] Ren Y, Jia L, Zhang Y, Zhang Z, Xue S, Yue S, and Du H 2022 *Phys. Rev. A* **106** 033123

[34] He Y L, Guo J, Gao F Y, and Liu X S 2022 *Phys. Rev. B* **105** 024305

[35] Shao T J, Lü L J, Liu J Q, and Bian X B 2020 *Phys. Rev. A* **101** 053421

[36] Qiao Y, Chen J, Zhou S, Chen J, Jiang S, and Yang Y 2024 *Chin. Phys. Lett.* **41** 014205

[37] Hu S Q and Meng S 2023 *Chin. Phys. Lett.* **40** 117801

[38] Nourbakhsh Z, Tancogne-Dejean N, Merdji H, and Rubio A 2021 *Phys. Rev. Applied* **15** 014013

[39] Zhong C L, Qiao B, Xu X R, Zhang Y X, Li X B, Zhang Y, Zhou C T, Zhu S P, and He X T 2020 *Phys. Rev. A* **101** 053814

[40] Qiao Y, Huo Y Q, Jiang S C, Yang Y J, and Chen J G 2022 *Opt. Express* **30** 9971

[41] Qiao Y, Chen J, Huo Y, Liang H, Yu R, Chen J, Liu W, Jiang S, and Yang Y 2023 *Phys. Rev. A* **107** 023523

[42] Li J, Zhang X, Fu S, Feng Y, Hu B, and Du H 2019 *Phys. Rev. A.* **100** 043404

[43] Qiao Y, Chen J, Li Z, Liu Y, Jiang S, Liu W, Yang Y, and Chen J 2024 *Opt. Lett* **49** 3986

[44] Qiao Y, Wang N, Jiang S, Yang Y, Chen J, and Dorfman K 2024 *Phys. Rev.B* **110** 075201

[45] Qian C, Jiang S C, Wu T, Weng H M, Yu C, and Lu R F 2024 *Phys. Rev.B* **109** 205401

[46] Jiang S, Yu C, Chen J, Huang Y, Lu R, and Lin C D 2020 *Phys. Rev. B* **102** 155201

[47] Yang Y J, Chen J G, Chi F P, Zhu Q R, Zhang H X, and Sun J Z 2007 *Chin. Phys. Lett.* **24** 1537